SAND2024-10528C

Effect of Silicon Photomultiplier Optical Crosstalk on Detection Performance in Organic Scintillators

J. Fritchie[a,*], J. Balajthy[b], M. Sweany[b], T. Weber[b], A. Di Fulvio[b]

[a] *Department of Nuclear, Plasma, and Radiological Engineering, University of Illinois, Urbana-Champaign,*
[b] *Sandia National Laboratory*

Abstract

This paper presents a method to reduce optical crosstalk (OCT) in a MicroFJ30035 silicon photomultiplier (SiPM) by ONSemi, which is a solid-state photon detector capable of detecting single photons. SiPMs are a promising alternative to vacuum photomultiplier tubes in radiation detection scenarios that require low-voltage power requirements, small form factor, and durability. However, the applicability of SiPMs in harsh environments is currently limited due to their temperature-dependent noise, which degrades their signal-to-noise ratio.

One of the main sources of noise in SiPMs is OCT, which arises when a photon is produced during an avalanche, and the resulting photon can then trigger another avalanche in neighboring pixels, leading to false counts. Therefore, reducing OCT is crucial to enhance the performance of SiPMs in high-temperature environments.

In this report, we explore a method to reduce OCT in 3mm x 3mm SiPMs by placing a series of Schott bandpass filters over the sensor of the SiPM. Filters with various spectral characteristics were tested on their abilities to suppress unwanted crosstalk signals while preserving the desired signal. We demonstrate the effectiveness of the filters by measuring the OCT in the SiPM before and after the filter installation and show a significant reduction in the OCT.

1. Background and Motivation

Scintillation detectors are widely used in various fields, including high-energy physics [1], medical imaging [2], and nuclear security [3]. These detectors convert the light emitted by the scintillating material into electrical signals, which are then measured to infer the properties of the incident radiation.

*Corresponding author. Tel.: +1 618 562 5475.
Email address: jwf2@illinois.edu (J. Fritchie)

Traditionally, vacuum photomultiplier tubes (PMTs) have been the detectors of choice for scintillation-based systems. However, they suffer from several limitations, such as high-voltage power requirements, large size, sensitivity to magnetic fields, and fragility, which can limit their use in certain applications. Silicon photomultipliers (SiPMs) offer a compelling alternative to PMTs, as they have lower-voltage power requirements, a smaller form factor, and are more robust.

SiPMs consist of an array of micro-cells, each operated in Geiger-mode, that are sensitive to light. When a photon enters a cell, it produces electron-hole pairs, which trigger an avalanche of charge amplification, resulting in a measurable electrical signal. SiPMs' small size and low power consumption make them attractive for use in portable radiation detectors [4], high-spatial resolution radiation trackers [5], and tomography systems [6].

However, SiPMs' noise is temperature-dependent, which can reduce their signal-to-noise ratio and limit their applicability in harsh environments. The main sources of noise in SiPMs are dark counts, optical crosstalk, and afterpulsing. Dark counts are thermally-induced electron-hole pairs that can trigger an avalanche in a micro-cell even in the absence of incident photons. Optical crosstalk occurs when a photon is produced during an avalanche, and the resulting photon can then trigger another avalanche in neighboring pixels, leading to false counts. Afterpulsing is the delayed release of charge from a micro-cell due to trapping of charge carriers in the cell's material.

To overcome these limitations, several approaches have been proposed, including temperature control systems [7] and gating techniques [8]. In this paper, we reduce optical crosstalk in a 3mm x 3mm SiPM by using different Schott bandpass filters placed over the sensor of the SiPM. This approach is simple, cost-effective, and does not require any modifications to the SiPM structure. We demonstrate the effectiveness of the method by measuring the optical crosstalk in a MicroFJ30035 SiPM before and after the filter installation and show a significant reduction in the crosstalk.

2. Methods

2.1. Experimental Methods

We began by characterizing the optical crosstalk (OCT) probability of a MircoFJ30035 SiPM in its unmodified state. The SiPM was placed inside a light-tight vacuum chamber with a modified lid, as shown in Figure 1, which included a flange for power and signal lines to pass through to the SiPM. The chamber was maintained at a vacuum of -0.6 Bar and a temperature of 19°C. To measure the SiPM's output signal, we connected it directly to a MiniCircuits ZFL-1000LN+ low-noise amplifier, which was then connected to a 14-bit 500-MSps DT5730 digitizer by CAEN technologies. All signal data was collected on a computer via USB.

We powered the SiPM with 5V of overvoltage and collected signal data for five minutes. However, the triggering frequency was over 1000 kHz, causing

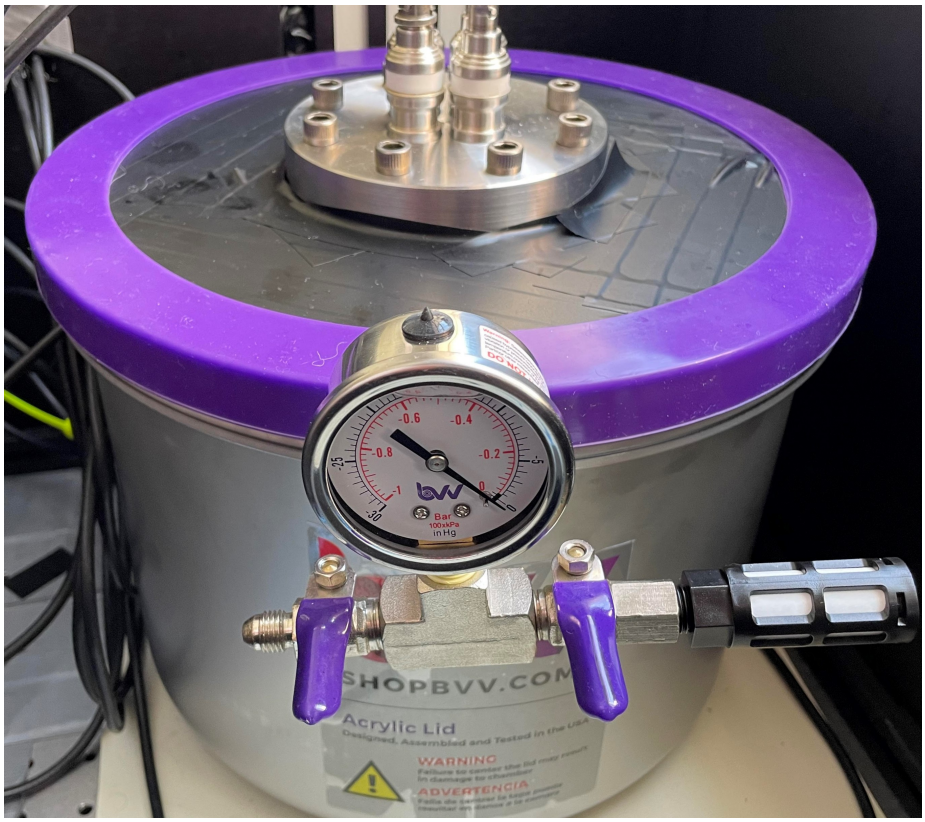

Figure 1: Vacuum chamber used for OCT measurement.

a buffer overflow in the digitizer. To solve this issue, we used a Fast Digital Detector Emulator to generate a 10 kHz 50% duty cycle TTL pulse, which triggered the digitizer to acquire signal data for a set acquisition window of 992 ns.

Before testing the SiPM with bandpass filters to reduce OCT, we removed the inductor and fast output connector. These modifications did not affect the performance of the SiPM, as confirmed by measurements taken before and after the modifications.

After placing a Semrock BrightLine Multiphoton FF01-520/70-2 Filter on top of the SiPM sensor, we conducted tests using Schott filters to evaluate their OCT reduction capabilities. The Semrock filter was used to reflect OCT-generated photons back at the sensor, in a manner similar to a scintillator. We tested four bandpass filters (KG2, UG5, BG39, and BG40) with different cutoff regions to assess their OCT reduction capabilities in different wavelength regions. Additionally, we used five longpass filters (N-WG280, OG590, RG695, RG850, and RG1000) with various transmittance regions. A schematic of this setup can be seen in Figure 2. Each bandpass filter was applied to the SiPM

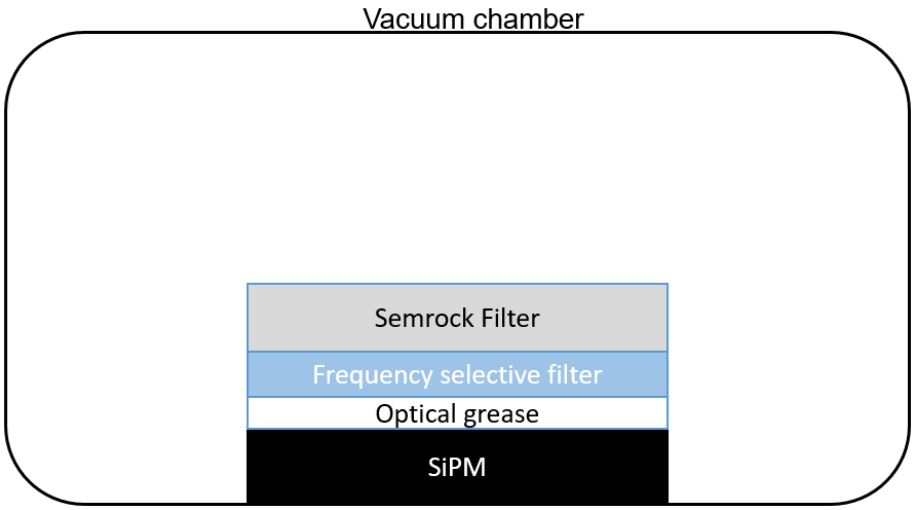

Figure 2: Schematic showing measurement setup.

surface using EJ-550 optical grease, which has a refractive index of 1.46.

2.2. Data Processing

We performed a pulse height analysis on the signals from the measurement acquisition. An example of a raw signal is displayed in Figure 3. The baseline was calculated as the mean of the first 7 samples. If there was a peak in the first 7 samples of the acquisition window, the window was ignored. The decay of the pulses was then removed, which improved the calculation of the pulse heights.

In each acquisition window, the mean of the six points preceding and including the minimum were subtracted from the signal. Then, the resulting trace was divided by the decay time of the pulse, which was set to 60 ns. Equation 1 represents this method

$$V_i = V_{Oi} + \frac{1}{\tau} + \sum_{j=1}^{j=i} V_{Oj} \times (t_j - t_{j-1}) \tag{1}$$

where $t_{j-1} = 0$ and $V_0 = V - V_{min}$. t is the time in nanoseconds, V is volts in millivolts, τ is the microcell recharge time of the SiPM, i represents the current sample, and j represents the previous samples.

A bandpass filter was applied to the decay-removed pulse with critical frequencies of 100 MHz and 30 MHz to more easily identify the peak sample. A peak finding algorithm found all peak samples in the bandpass filtered trace above a threshold of 2 mV. An example of this method is shown in Figure 4. The pulse heights were recorded for all acquisition windows for each measurement. The resulting pulse heights were plotted into a histogram as in Figure 5. The first peak contains all the 1 photoelectron (p.e.) peaks. Single p.e. peaks

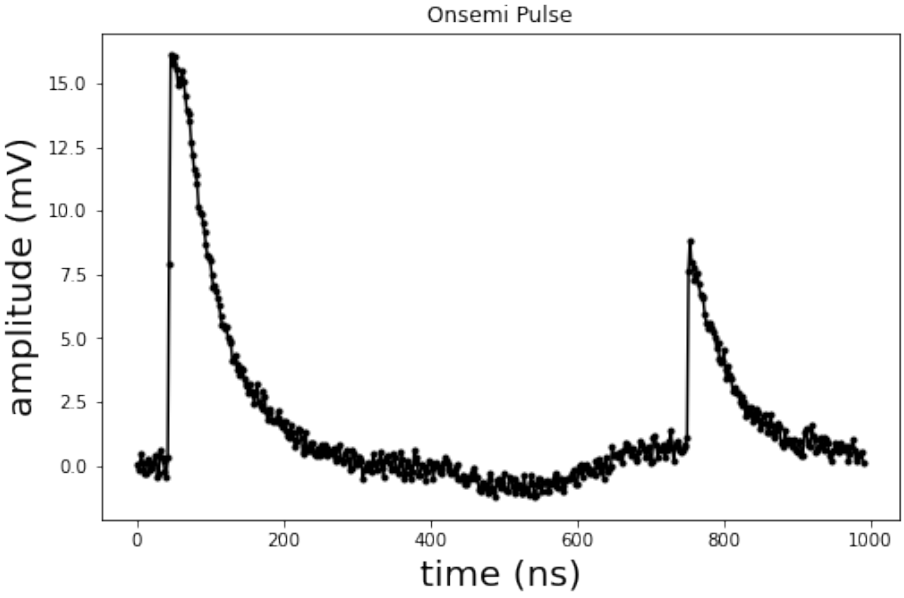

Figure 3: An example of the raw signal in one acquisition window.

result from an avalanche from a single microcell. In this case, the avalanches were caused by dark counts. Beyond the first p.e. peak are higher order p.e. peaks. These higher order p.e. peaks are caused by prompt OCT. The OCT photons trigger the surrounding microcells simultaneously to the originally triggered microcell, resulting in peaks with higher amplitude.

The dark counts were counted as the area under the 1 p.e. peak in 5 while the area under the subsequent peaks were counted as OCT events. The OCT probability was calculated using Equation 2

$$OCT_p = \frac{OCT}{DC + OCT} * 100 \tag{2}$$

where OCT_p is the OCT probability, OCT is the number of OCT events, and DC is the number of dark count events.

3. Results

The bandpass filters tested reduced optical crosstalk probability in the SiPMs between 4.8% and 6.1% from the 23.7% measured with the Semrock filter placed on the sensor to mimick the presence of a detector's surface. The full results are listed in Table 1.

Similarly to [9], the decrease in OCT probability seen in the LPFs suggests that wavelengths between 600 nm and 1000 nm contribute primarily to OCT. This is an expected result, as the photons generated during OCT events are

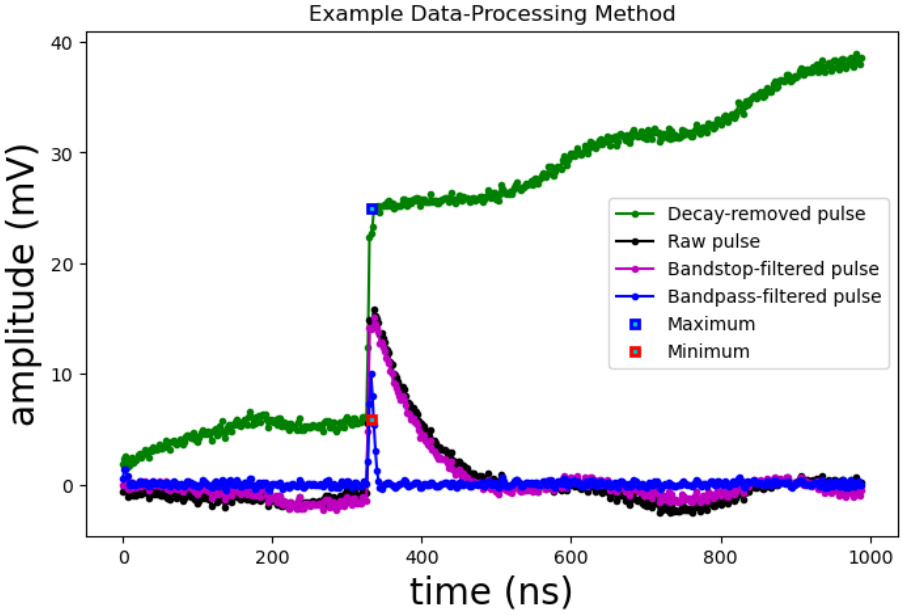

Figure 4: An example of the data-processing method. The calculated maximum is the blue square, and the minimum is the red square.

Table 1: Measured OCT probability for different filters. All measurements following the FF01-520/70-2 include it resting above the longpass and bandpass filters.

Filter Name	OCT Probability	Wavelength Selection
Bare	21.4%	
$FF01-520/70-25$	23.7%	Transmittance band: 485nm-555nm
$N-WG280$	18.7%	200nm-250nm
$OG590$	18.9%	200nm-550nm
$RG695$	18.6%	200nm-650nm
$RG850$	18.1%	200nm-700nm
$RG1000$	17.8%	200nm-700nm
$UG5$	17.8%	400nm-600nm
$BG39$	17.6%	700nm-1000nm
$BG40$	17.6%	700nm-1000nm
$KG2$	18.1%	800nm-1200nm

often near infrared wavelength [10]. The BPFs also show significant reduction in OCT probability, with the greatest decreases in the BG39 and BG40. The selection of suitable filters can potentially be a strategy to reduce one of the primary sources of noise in SiPM signals, i.e. OCT, and therefore increase the signal-to-noise ratio.

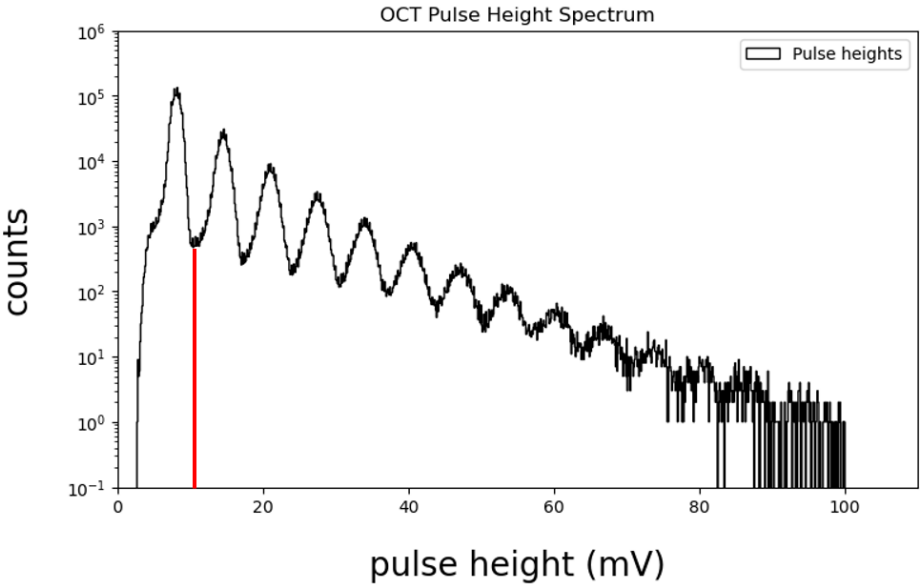

Figure 5: A pulse height spectrum acquired from an OCT measurement. The red line shows the minimum between the 1 and 2 p.e. peaks. All peaks to the left are counted as dark counts while those on the right are considered optical crosstalk.

References

[1] P. Russo, Gamma-ray measurements of holdup plant-wide: application guide for portable, generalized approach, LA-14206 (2005).

[2] G. Llosá, J. Barrio, J. Cabello, C. Lacasta, J. F. Oliver, M. Rafecas, V. Stankova, C. Solaz, M. G. Bisogni, A. Del Guerra, Detectors based on silicon photomultiplier arrays for medical imaging applications, in: 2011 2nd International Conference on Advancements in Nuclear Instrumentation, Measurement Methods and their Applications, 2011, pp. 1–5. doi:10.1109/ANIMMA.2011.6172967.

[3] M. A. Wonders, D. L. Chichester, M. Flaska, Characterization of new-generation silicon photomultipliers for nuclear security applications., EPJ Web of Conferences 170 (2018) 1 – 6.
URL http://www.library.illinois.edu.proxy2.library.illinois.edu/proxy/go.php?url=https://search-ebscohost-com.proxy2.library.illinois.edu/login.aspx?direct=true&db=asn&AN=127305648&site=eds-live&scope=site

[4] P. R. Menge, J. Lejay, V. Ouspenski, Design and performance of a compact cs2lilabr6(ce) neutron/gamma detector using silicon photomultipliers., 2015 IEEE Nuclear Science Symposium and Medical Imaging Conference (NSS/MIC), Nuclear Science Symposium and Medical Imaging Conference

(NSS/MIC), 2015 IEEE (2015) 1 – 5.
URL https://proxy2.library.illinois.edu/login?url=https://search.ebscohost.com/login.aspx?direct=true&db=edseee&AN=edseee.7581858&site=eds-live&scope=site

[5] Z. Liu, M. Niu, Z. Kuang, N. Ren, S. Wu, L. Cong, X. Wang, Z. Sang, C. Williams, Y. Yang, High resolution detectors for whole-body pet scanners by using dual-ended readout., EJNMMI Physics 9 (1) (2022) 1 – 18.
URL https://proxy2.library.illinois.edu/login?url=https://search.ebscohost.com/login.aspx?direct=true&db=asn&AN=156445446&site=eds-live&scope=site

[6] . . Seo, M. (1, . . Park, H. (1, . . . Lee, J.S. (2, Evaluation of large[U+2010]area silicon photomultiplier arrays for positron emission tomography systems., Electronics (Switzerland) 10 (6) (2021) 1–10 – 10.
URL https://proxy2.library.illinois.edu/login?url=https://search.ebscohost.com/login.aspx?direct=true&db=edselc&AN=edselc.2-52.0-85102571580&site=eds-live&scope=site

[7] R. Raylman, A. Stolin, Immersion cooling of silicon photomultipliers (sipm) for nuclear medicine imaging applications, Radiation Measurements 85 (2016) 111–115. doi:https://doi.org/10.1016/j.radmeas.2015.12.043.
URL https://www.sciencedirect.com/science/article/pii/S1350448715301220

[8] G. Chesi, L. Malinverno, A. Allevi, R. Santoro, M. Caccia, A. Martemiyanov, M. Bondani, Optimizing silicon photomultipliers for quantum optics, Scientific Reports 9 (1) (2019) 1–12.

[9] T. Masuda, D. G. Ang, N. R. Hutzler, C. Meisenhelder, N. Sasao, S. Uetake, X. Wu, D. DeMille, G. Gabrielse, J. M. Doyle, K. Yoshimura, Suppression of the optical crosstalk in a multi-channel silicon photomultiplier array, Opt. Express 29 (11) (2021) 16914–16926. doi:10.1364/OE.424460.
URL https://opg.optica.org/oe/abstract.cfm?URI=oe-29-11-16914

[10] R. Mirzoyan, R. Kosyra, H.-G. Moser, Light emission in si avalanches, Nuclear Instruments and Methods in Physics Research Section A: Accelerators, Spectrometers, Detectors and Associated Equipment 610 (1) (2009) 98–100, new Developments In Photodetection NDIP08. doi:https://doi.org/10.1016/j.nima.2009.05.081.
URL https://www.sciencedirect.com/science/article/pii/S0168900209010377